Orbit and Formation Control for the Next Generation Gravity Mission ⋆

L. Colangelo * **E. Canuto** * **L. Massotti** ** **C. Novara** *
M. A. Lotufo *

* *Department of Control and Computer Engineering, Politecnico di Torino, 10129 Torino, Italy (luigi.colangelo@polito.it)*
** *Earth Observation Programmes Department - Future Missions Division (EOP-SF), ESA-Estec, NL-2200 Noordwijk, The Netherlands (Luca.Massotti@esa.int)*

Abstract: This paper focuses on the orbit and formation control for the Next Generation Gravity Mission (NGGM), under study at the European Space Agency. In our past study, an innovative integrated orbit/formation model (IFC) has been designed, introducing a novel set of Hill-type equations. The aim of this study is the refinement and the enhancement of the IFC architecture. The proposed solution is based on a modified state predictor plus an extended hierarchical and multi-rate structure of the control law, with respect to the preliminary design. Care was taken in the control design to reduce as much as possible the demanded extra-thrust effort. This improved control strategy has been shown to be far less sensitive to the initial formation perturbations as well as capable of keeping the formation variables stable within the required band, all over the 10-year mission, through a low-thrust authority in the order of few milli-newtons.

Keywords: Spacecraft Formation Flying, Orbit Control, Formation Control, Low-Earth Formation, Gravimetry

1. INTRODUCTION

Post ESA's GOCE (Gravity Field and Steady-State Ocean Circulation Explorer), space Earth gravimetry missions will rely on a formation of satellites, flying in loose formation in a low Earth orbit, acting as proof masses immersed in the Earth gravity field and on the measurement of their distance fluctuations, encoding the gravity anomalies. Indeed, the performance level of gravity missions can be substantially increased by adding a formation control to long-distance distributed space systems as in GRACE (Gravity Recovery And Climate Experiment), in the order of 100 km distance, but at a lower altitude (300 to 400 km). Such a mission configuration requires that each satellite is drag-free and completed by an accurate distance measurement system. As a result, the Next Generation Gravity Mission (NGGM), under study at the European Space Agency, will consist in a two-satellite long-distance formation, placed in a low near-polar orbit. Each satellite will be controlled to be drag-free, while laser interferometry will ensure the satellite-to-satellite tracking.

This paper focuses on the orbit and formation control for the NGGM mission, whose aim is the orbit and formation long-term stability (> 10 years). One of the most relevant contribution of this paper is the refinement and the enhancement of the integrated orbit and formation control (IFC) architecture described by Canuto et al. (2014a), so to overcome possible drift and stability issues due to a large envelope of the formation initial perturbations. As in Canuto et al. (2014a), the orbit and formation dynamics is formulated as a special kind of Clohessy-Wiltshire (CW) equations [Wiltshire and Clohessy (1960)]. Such formulation is based on the definition of a peculiar formation reference frame (the formation local orbital frame, FLOF) and the formation triangle.

There are many possible ways to define the dynamics of a satellite formation and to control it. Three main approaches may be found in literature [Ren and Beard (2004)]: leader-follower, behavioural, and virtual structure. The stability and the accurate formation dynamics free response has also been largely investigated. For small formations, the effects of the non-linear terms are negligible, but the effects of the gravitational perturbations and the reference orbit eccentricity are often significant [Alfriend et al. (2000), Schaub and Alfriend (2000)]. Hence, attention has been paid to include in the model generic gravity potential terms as in Guibout and Scheeres (2012) or to extend relative orbit motion to eccentric orbits as in Yamanaka and Ankersen (2002). There have also been analyses to develop formations that are insensitive to differential J2 disturbances, based on non-linear dynamic models [Schaub and Alfriend (2000)]. At this proposal, Schaub and Alfriend (2000) suggest that by specifying the relative orbit geometry in mean elements the true relative spacecraft motion does not deviate from the prescribed relative orbit geometry. However this method has been

⋆ Part of this research was carried out within the study *Next Generation Gravity Mission (NGGM): AOCS Solutions and Technologies study* and within the ESA Networking Partner Initiative (NPI) PhD project *Laser Metrology Spacecraft Formation* (Ref. 4000109653/13/NL/MH) funded by the European Space Agency; Thales Alenia Space Italy (Turin) being the prime contractor.

found to be too weak in some particular orbit conditions by Schaub et al. (2000), which study methods to reestablish these J2 invariant relative orbits by feedback. Another way to address the description of proximity relative motion for formation or rendezvous mission is to develop the state transition matrix, even for eccentric orbits, both in dependence of time [Melton (2000)] or true anomaly [Inalhan et al. (2002), Yamanaka and Ankersen (2002)]. On the other hand, care must be taken in employing CW perturbation equations for control design in the case of a long-distance formation baseline, since significant non-linear gravity terms are neglected. For instance, Alfriend et al. (2000) used state-transition matrices to account the orbit eccentricity and the gravity perturbations. The approach adopted in this paper is based on the Embedded Model Control (EMC) design [Canuto et al. (2014c), Canuto et al. (2014b)], which calls for a hierarchical and multi-rate control unit around the real-time internal model of the satellite formation controllable dynamics. The embedded model control technique fully solves this sort of problems through a simple but effective disturbance estimation dynamics. Hence, the main advantages, inter alia, consist in both being free to adopt a simplified internal model and directly rejecting the perturbations from the LTI model, reducing the required thrust level and fuel consumption.

This paper starts with some concepts about the NGGM mission requirements and the architecture of the control design. After this brief outline, the paper describes the formation triangle dynamics model, introducing the FLOF frame. The discrete-time (DT) final equations of the formation internal model are provided. As a consequence, leveraging the EMC design, the state predictor and the control law are built on and interfaced to the internal model. Finally, some preliminary simulated results proving control performances are provided.

2. NGGM MISSION REQUIREMENTS AND CONTROL ARCHITECTURE

The NGGM mission fundamental observable is the distance variation between the two CoMs. However, within the total distance variation, only the small fraction due to the gravity acceleration (i.e. the Earth gravity field anomalies effect) is of interest. Consequently, the NGGM mission concept leverages a two-satellite formation, ideally drag-free and flying as test masses in the Earth gravity field. Such a pair of distant drag-free satellites acts as a sort of gradiometer, with a very long baseline ($\approx 200\,\mathrm{km}$).

From the orbit and formation control perspective, such a drag-free formation implies that no stringent requirements apply to the formation control. Indeed, in principle the two satellites, while acting as proof-masses, must be left free to move under the action of the Earth gravity field. However, an ideal drag-free control is not possible, mainly due to the accelerometer errors (e.g. bias, drift). Hence, an orbit and formation control is needed.

The Table 1 lists the main requirements driving the control design in the science mode of the NGGM mission. Note that the formation requirements have been split into distance, radial and lateral variations with respect to a nominal circular orbit; expressed as a percentage of the nominal inter-satellite distance. Concerning the attitude and orbit control system (AOCS) design, the main design principles are:

Table 1. NGGM mission science control mode: main performance requirements for the AOCS.

Performance variable	**Bound**	**Unit**
Drag-free control		
CoM acceleration (PSD in MBW)	0.01	$\mu m/s^2/\sqrt{Hz}$
CoM acceleration	1	$\mu m/s^2$
Orbit and formation control		
Formation distance variation	5	% (distance)
Formation lateral variation	1	% (distance)
Formation radial variation	2	% (distance)

Embedded Model Control AOCS is designed around a simplified, discrete-time model of the spacecraft and formation dynamics to be embedded in the control unit. This embedded model consists of the controllable dynamics and of the disturbance dynamics. The disturbance dynamics is in charge of estimating a wide range of unknown model errors as drag-free residuals, parametric uncertainties, cross couplings and neglected non-linearities.

Integrated orbit and formation control The orbit and formation control design is driven by an innovative approach to multi-satellite formation and orbit control. Such innovative approach is based on the integration of orbit and formation dynamics and control through the formation triangle concept and leads to new Hill-type equations (see Canuto et al. (2014a) and Section 3).

Multi-hierarchical control Control tasks are carried out via a multi-hierarchical control design, as described later in this section.

Frequency coordination The drag-free control and the formation control are actuated at different frequency bands. This is deemed necessary in order to prevent any possible interference among inner/outer loops control functions and to coordinate properly the several tasks of the control design.

The higher-level block-diagram of the AOCS architecture, in science phase, is sketched in Fig. 1. From the control architecture perspective, formation and drag-free control are designed in a hierarchical way. Indeed, the integrated orbit and formation control is an outer loop which provides the long-term reference accelerations to be tracked by drag-free control. As a result, in Fig. 1, loops 3, 4, and 5 pertain to the enhanced integrated orbit/formation control plus the linear drag-free. The loops 4 and 5, addressing the control of the formation position (loop 4) and the formation rate (loop 5), are actuated at different and appropriate frequency bands. Indeed, the low-frequency formation position control (loop 4) employs orbital-averaged measurements in order to filter out any component of gravitational nature and the command is actuated at the orbit frequency (close to $0.2\,\mathrm{mHz}$). Further, a damping control function (loop 5) has been added in the present enhanced IFC configuration. Such damping control, concerning the formation linear rate variables, is actuated at an higher frequency and it has been proved to be necessary to ensure the orbit and formation BIBO stability. This sub-hierarchical structure within the orbit and formation control is the main novelty with respect to

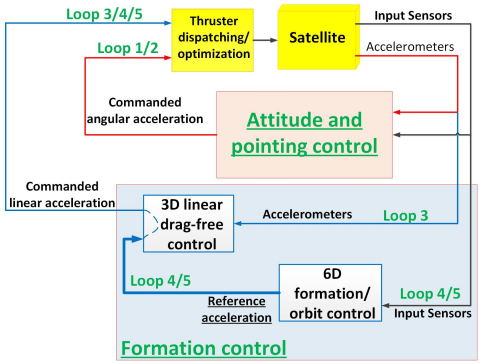

Fig. 1. Higher-level block diagram of the AOCS architecture for the NGGM science mode.

what was presented in Canuto et al. (2014a), leading to the enhanced IFC architecture which has been proved to improve substantially the control performance level as well as the stability of the formation triangle.

3. INTEGRATED ORBIT AND FORMATION DYNAMICS

In this section, the main focus will be on the enhanced integrated orbit and formation dynamics, focusing on the inline formation type, in which the satellites follow the same orbital path, with different true anomalies. Due to the drag-free control action, the orbit/formation model has been designed by assuming that the gravity periodic components are the only source of acceleration. The rationale behind our novel set of Hill-type equations is the integration into a unique model of the orbit and formation dynamics and control, through the formation triangle concept (Fig. 2 and (Canuto et al., 2014a)). This integrated model is based on the the formation local orbital frame (FLOF), depicted in Fig. 2. The FLOF is materialized by the GNSS range measurements, as soon as the GNSS receivers become operational, and its three axes are defined as follows:

$$\mathbf{o}_1 = \frac{\Delta\mathbf{r}}{d}, \quad \mathbf{o}_2 = \frac{\frac{\mathbf{r}}{r} \times \mathbf{o}_1}{|\frac{\mathbf{r}}{r} \times \mathbf{o}_1|}, \quad \mathbf{o}_3 = \mathbf{o}_1 \times \mathbf{o}_2 \tag{1}$$

where $\mathbf{r} = (\mathbf{r}_1 + \mathbf{r}_2)/2$ is the mean formation radius, $\mathbf{\Delta r} = (\mathbf{r}_1 - \mathbf{r}_2)$ is the satellite relative position, $d = |\mathbf{\Delta r}|$ is the inter-satellite distance. Following the FLOF definition, the formation triangle, whose edges join the two satellite CoMs and the Earth CoM, is another paramount element for the integrated orbit and formation modelling (as derived in Canuto et al. (2014a)). Satellite-to-satellite distance variations are measured along the satellite-to-satellite line (SSL in Fig. 2). Given a proper attitude and pointing control, intended to keep aligned the satellites optical axis, the SSL is defined as the line connecting the CoM of the satellites; aligned with the first FLOF axis. Figure 2 provides also a sketched visualization of the orbit perturbations adopted in the orbit/formation modelling as well as the formation triangle DoFs. Indeed, orbit/formation dynamics is expressed through a combination of Cartesian and angular perturbations (triangle angular rotations), defined through the FLOF frame. Given a reference orbit (i.e. a reference sphere) with nominal radius r_{nom} and the nominal inter-satellite distance d_{nom}, the three adopted Cartesian perturbations are: (i) the distance variation δd, (ii) the formation mean radius deviation (along the SSL) δr_x, (iii) the mean altitude variation δr_z, viz.

$$\begin{aligned} \Delta\mathbf{r} &= (d_{nom} + \delta d) \\ \mathbf{r} = r_z\mathbf{o}_3 + r_x\mathbf{o}_1 &= (r_{nom} + \delta r_z)\mathbf{o}_3 + \delta r_x\mathbf{o}_1. \end{aligned} \tag{2}$$

In addition, the formation triangle has three further DoFs consisting in the three components of the FLOF angular rate vector with the relative angular perturbations. Hence, the integrated orbit and formation dynamics is based on the differential equations of these six perturbations. Such equations were built by combining the kinematics equations involving the six selected perturbations with the formation triangle dynamics (as explained in Canuto et al. (2014a)). The final perturbation equations were used for the control design after having been linearised around the equilibrium point. It is worth to underline that gravity and gravity gradient terms have been expressed in series expansion at the first order (i.e. spherical gravity). Indeed, all the higher order terms, from J2 on, have been treated as disturbances belonging to the external acceleration term affecting the formation dynamics. Such a model linearisation perfectly fits with the Embedded Model Control technique. Indeed, EMC allows one to recover and reject in the control law all the non-explicitly modelled effects, like the J2 and higher order terms, through a stochastic and parameter-free disturbance dynamics, driven by the model error. As a result, formation/orbit dynamics can be expressed in terms of the perturbations of a nominal formation affected by the spherical gravity, having zero-eccentricity orbit, and defined by nominal inter-satellite distance, radius, and angular rate.

Define the state vector as $\mathbf{x} = [\mathbf{r}_t \quad \mathbf{w}]^T = [\rho_x \quad \rho_z \quad \delta d \quad d_{nom}\delta\theta \quad w_x \quad w_z \quad w_d \quad w_y]^T$, where $\rho_x = \alpha\delta r_x$ and $\rho_z = \alpha\delta r_z$. The linearised state equations are the following:

$$\begin{bmatrix} \dot{\mathbf{r}}_t \\ \dot{\mathbf{w}} \end{bmatrix}(t) = \begin{bmatrix} 0 & I\omega_{nom} \\ A_{21} & A_{22} \end{bmatrix} \begin{bmatrix} \mathbf{r}_t \\ \mathbf{w} \end{bmatrix}(t) + \begin{bmatrix} 0 \\ B_2 \end{bmatrix} \mathbf{u}(t), \quad \begin{bmatrix} \mathbf{r}_t \\ \mathbf{w} \end{bmatrix}(0) = \begin{bmatrix} \mathbf{r}_{t0} \\ \mathbf{w}_0 \end{bmatrix}$$

$$\mathbf{y}(t) = \begin{bmatrix} I & 0 \end{bmatrix} \begin{bmatrix} \mathbf{r}_t \\ \mathbf{w} \end{bmatrix}(t)$$

$$A_{21} = 3\omega_{nom} \begin{bmatrix} 1 & 0 & 0 & 0 \\ 0 & 1 & 0 & 0 \\ 0 & 1 & 0 & 0 \\ -1 & 0 & 0 & 0 \end{bmatrix}, \quad A_{22} = 2\omega_{nom} \begin{bmatrix} 0 & -1 & 1 & 0 \\ 1 & 0 & 0 & 1 \\ 0 & 0 & 0 & 1 \\ 0 & 0 & -1 & 0 \end{bmatrix} \tag{3}$$

$$B_2 = \begin{bmatrix} \alpha & 0 & 0 & 1 \\ 0 & \alpha & 0 & 0 \\ 0 & 0 & 1 & 0 \\ 0 & 0 & 0 & -1 \end{bmatrix} \omega_{nom}$$

where ω_{nom} is the nominal orbital angular rate, $\alpha = d_{nom}/r_{nom}$ is an adimensional scale factor, $d_{nom}\delta\theta$ is the longitudinal perturbation, $\mathbf{x}$ represents the formation perturbations while $\mathbf{w}$ is the normalized formation rate perturbations sub-vector. The preliminary version of the IFC design was based on the model described by equation (3). Notwithstanding extensive simulations have been showing the effectiveness of the model in (3) for the control design, the preliminary IFC seems to show some criticality in some conditions. Indeed, given the very low thrust level constraining the NGGM control design, stability and drift issues seem to affect some formation variable in case of a set of initial conditions non optimal for starting the NGGM mission science phase. Specifically, issues of this kind can arise after: (i) poor/missing formation and orbit acquisition, (i) pre-science control modes transition. Hence, the rationale behind the enhanced IFC pursues an increased control robustness, when the formation starts the scientific control mode outside a given envelope around the equilibrium point. Therefore, the preliminary IFC model

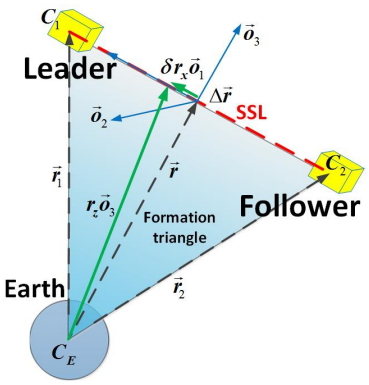

Fig. 2. The formation triangle and the Formation Local Orbital Frame (FLOF).

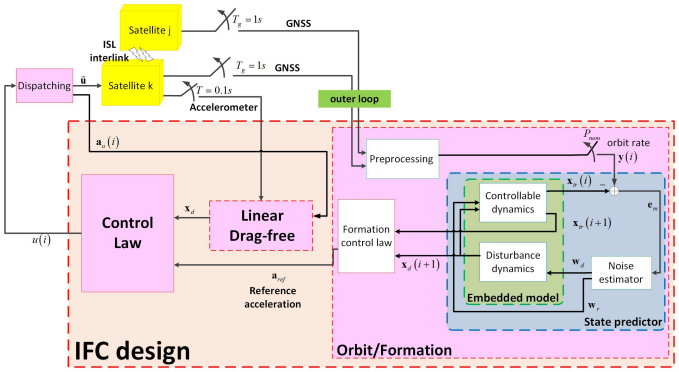

Fig. 3. The IFC design: sensors to actuators chain.

has been studied and then transformed in order to: (i) improve its capability of managing the satellite orbit initial perturbations, (ii) supporting the control law in ensuring BIBO stability of the formation variables. The transformation of the perturbed formation state equations was driven by the analysis of the free response of the original model in (3), given a certain set of initial conditions. Indeed, the free response, similar to the Hill's case, includes a pair of diverging components affecting the distance variation δd and the longitudinal orbital perturbation $d_{nom}\delta\theta$. In addition, the free response presents constant terms (biases) affecting two other state variables (ρ_x and ρ_z). The idea is to cancel the free response divergence by controlling to zero the factors of the two drifting terms. Such drifting factors are linked to the initial conditions of the linear combinations of some state variables of (3). Hence, the state of the original model in (3) was transformed by combining linearly some of its state variables (see d_w and θ_w in (4)) to be controlled to zero. Then, leveraging two further linear combinations of the state variables in (3), also the biased term of the free response can be forced to zero (introducing the two further combined states ρ_{xw} and ρ_{zw} in (4)), thus making the free response zero-mean and bounded. As a consequence, transforming the model in (3) according to the new combined state variables, a new set of state equations is obtained.
The state vector of the transformed model reads:

$$\mathbf{x}_{tr} = \begin{bmatrix} \mathbf{r}_w \\ \mathbf{w} \end{bmatrix} = [\rho_{xw} \quad \rho_{zw} \quad d_w \quad \theta_w \quad w_x \quad w_z \quad w_d \quad w_y]^T, \tag{4}$$

where $\rho_{xw} = \rho_x + (w_d - w_z)/2$, $\rho_{zw} = \rho_z + (w_y + w_x)/2$, $d_w = \delta d + 3\rho_z + 2w_y$ and $\theta_w = d_{nom}\delta\theta - 3\rho_x - 2w_d$. It is worth to notice that the formation rate sub-vector does not change after the transformation. As a further step, the final transformed LTI continuous system is made discrete time to be implemented within a digital control unit.

At this point, according to the EMC design, the embedded model to be coded directly into the control unit can be built. The embedded model encompasses the controllable model (i.e. the ZOH DT version of transformed (3)) completed by a purely stochastic and parameter-free disturbance dynamics, to describe the secular components (bias and drift) of the unknown disturbances. The integrated orbit/formation embedded model with a first-order disturbance dynamics is reported in (5). To build the controllable dynamics part, all the uncontrollable variables as the longitudinal perturbation and the formation rates have been dropped, since we are only interested in the control of the formation triangle position variables.

$$\begin{bmatrix} \mathbf{r}_w \\ \mathbf{x}_d \end{bmatrix}(i+1) = \begin{bmatrix} A_w & I \\ 0 & I \end{bmatrix}\begin{bmatrix} \mathbf{r}_w \\ \mathbf{x}_d \end{bmatrix}(i) + \begin{bmatrix} B_w \\ 0 \end{bmatrix}\mathbf{u}(i) + \begin{bmatrix} \mathbf{w}_r \\ \mathbf{w}_d \end{bmatrix},$$
$$\begin{bmatrix} \mathbf{r}_w \\ \mathbf{x}_d \end{bmatrix}(0) = \begin{bmatrix} \mathbf{r}_{w0} \\ \mathbf{x}_{d0} \end{bmatrix} \quad \mathbf{y}(i) = \begin{bmatrix} I & 0 \end{bmatrix}\begin{bmatrix} \mathbf{r}_w \\ \mathbf{x}_d \end{bmatrix}(i) + \mathbf{e}_m(i)$$
$$A_w = \begin{bmatrix} 1 & 0 & 0 \\ 0 & 1 & 0 \\ -12\pi & 0 & 1 \end{bmatrix}, B_w = \begin{bmatrix} 0 & -\alpha/2 & 1/2 & 0 \\ \alpha/2 & 0 & 0 & 0 \\ 0 & 3\pi\alpha & -3\pi & -2 \end{bmatrix}\frac{T_0}{\omega_{nom}} \tag{5}$$

In (5), $\mathbf{r}_w$ is the controllable state vector (comprising the three states relatively to the distance variations, the mean altitude and formation mean radius deviation), $\mathbf{x}_d$ is the disturbance state (expressing bias and drift of the accelerometer), while $\mathbf{w}_r$ and $\mathbf{w}_d$ components play the role of arbitrary, but bounded signals, to be kept as unpredictable and zero-mean. The vector $\mathbf{e}_m$ is the model error which encompasses measurement errors and the effect of neglected dynamics. Finally, the loop is closed by adding to the embedded model a static noise estimator (described by (6)), as in standard state observers. Each gain matrix L_i is diagonal, because the state equation is decoupled and the disturbance stochastic model further favors decoupling in presence of hidden coupling due to neglected non-linearities. In this way a complete state predictor is build.

$$\mathbf{w} = L\mathbf{e}_m, \qquad L = \begin{bmatrix} L_x & 0 \\ 0 & L_z \end{bmatrix} \tag{6}$$

As last step, the scalar gains on the diagonal of matrix L were tuned by fixing three pairs of closed-loop eigenvalues with a BW close to the orbital frequency, in order to allow a fast disturbance prediction. The Fig. 3 provides a simplified representation of the chain from sensors to actuators including the state predictor, encompassing embedded model and noise estimator, and its interface with the formation control law (to be described in Section 4) and the plant. In Fig. 3 is also clarified the structure of the embedded model.

4. ORBIT AND FORMATION CONTROL

The preliminary version of the integrated formation and orbit control (Canuto et al. (2014a)) was designed for stabilizing only the low-frequency components of the orbit and formation position variables: the mean altitude, the formation mean radius deviation and the inter-satellite distance. However, as above mentioned, some simulated

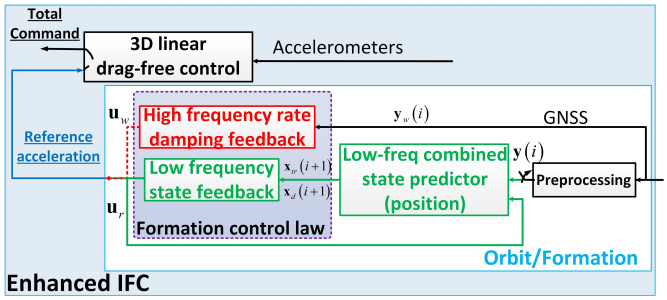

Fig. 4. Higher-level block diagram of the enhanced IFC architecture.

scenarios showed that such preliminary control strategy presented a drawback. In practice, the formation rate variables become uncontrollable by the low-frequency control of the DT IFC in (5) when closing the loops in some orbital conditions and affect the controllable variables stability. Therefore, orbit and formation stabilization, through the designed low-frequency (orbital) formation position feedback, has been proven to be guaranteed only for a certain envelope of formation initial perturbations.

The proposed solution is based on an extended hierarchical and multi-rate structure of the control law, providing the enhanced IFC architecture. Differently from the preliminary IFC, a further feedback loop has been added, involving the formation rate variables and aiming at ensuring their stability. This further feedback, a sort of rate damping control, operates at the time unit of the navigation data and damps suitably the formation rates components which have been found to affect the formation stability. In our implementation, in principle, the final enhanced IFC control architecture is in line with the typical servo positioning control architecture, leveraging an inner and fast rate damping loop. This enhanced IFC has been proved to ensures to a great extent the stability of the formation triangle variables of the inline formation within the required band, through a very low-thrust authority. On the other hand, in a solution of this kind the rate feedback must be carefully designed and optimised. Indeed, since this damping control loop is fully deployed from the very first moments of the mission science mode, our enhanced architecture may demand for a thrust authority larger than allowed. Figure 4 shows the higher-level block diagram of the enhanced IFC architecture. It is possible to notice the multi-loop structure of the formation control law block. As a design result, the enhanced IFC is a combination of two different control strategies actuating at very different time units.

First of all, the high-frequency rate damping control loop is directly fed by formation rates measurements, obtained from the navigation data, without any state predictor. Thus, the rate damping feedback command, helping in stabilising the systems, can be expressed as:

$$\begin{aligned} &\mathbf{u}_w = -B_2^{-1} K_w \mathbf{y}_w, \\ \text{where} \quad &K_w = \omega_{nom} diag\{\zeta_x, \zeta_z, \zeta_d, \zeta_w\}, \\ &\zeta_d << 1, \qquad \zeta_x = \zeta_z = \zeta_w = 0. \end{aligned} \tag{7}$$

In (7), $\mathbf{y}_w$ are the formation rate variable measurements, K_w is the feedback gain matrix, B_d^{-1} is the pseudo-inverse of the command matrix, ζ_i are the rate feedback gains, to be tuned to a value that guarantees formation stability and minimal thrust effort.

Secondly, the low-frequency state feedback operates at the orbital frequency and stabilizes the long-term perturbed dynamics of the formation triangle. Such control loop includes the low-frequency state predictor described in (5), in Section 3. Therefore, the low-frequency position feedback, at the orbital sampling step, reads:

$$\begin{aligned} &\mathbf{u}_r = -B_w^{-1}(K_r \mathbf{r}_w + \mathbf{x}_d), \\ \text{where} \quad &K_r = \begin{bmatrix} \gamma_x & 0 & 0 \\ 0 & \gamma_z & 0 \\ -12\pi & 0 & \gamma_d \end{bmatrix}. \end{aligned} \tag{8}$$

In (8), $\mathbf{x}_d$ is the disturbance state prediction of (5) to be rejected, $\mathbf{r}_w$ is the vector of the predicted combined formation variables, K_r is the feedback gain matrix, B_r^{-1} is the pseudo inverse of the command matrix as in (5). The reference part of the command is not explicitly reported in (8) because the state variables are regulated to zero, being defined as perturbations with respect to the nominal value.

As further design step, a preliminary closed loop tuning of the gains in (7) and (8), ensuring long-term stability as well as keeping at a minimum value the thrust authority, was pursued via pole-placement procedure. The selected gains were refined via simulation, while an accurate stability analysis of the closed-loop system will be performed as a further step of the work, to refine and evaluate the control unit performances. As a result, it appears that only few formation rate variables must be fed back in the rate damping control, to keep at a minimum the extra thrust authority required with respect to the only-low-frequency control strategy. A preliminary choice of the variables to be damped has been made by considering the most representative and typical inline long-run scenarios as provided by the preliminary mission studies. Specifically, only the ζ_d gain, damping the velocity of the distance, has been set different from zero ($\zeta_d = 2.8e{-}7$). Afterwards, the low-frequency control eigenvalues were tuned directly on the low-frequency state equations (5), which are derived by assuming zero damping. Eigenvalues not larger than 0.1 (time constant equal to ten times the orbit period) have been shown to be unaffected by inner rate damping feedback.

5. PRELIMINARY SIMULATED RESULTS

In this section will be shown some relevant simulated results obtained through a high-fidelity mission simulator. The science-phase AOCS includes linear and angular drag-free, attitude and pointing control and force/torque dispatching to an eight-thruster assembly. From the environment perspective, the first 32 harmonics of the Earth gravity field spherical expansion have been simulated together with an Oersted geomagnetic field model (order 18) and mean solar activity conditions. Finally, all the sensor and actuator noises are active. The reference inter-satellite distance has been fixed to 200 km.

Figure 5 shows the unilateral spectral density of the linear acceleration residuals versus the performance requirement. Such PSD has been computed on the whole residual profile including transient, which explains the low-frequency overshoot. Figure 6 shows the simulated total linear command, which includes linear drag-free command, orbit and

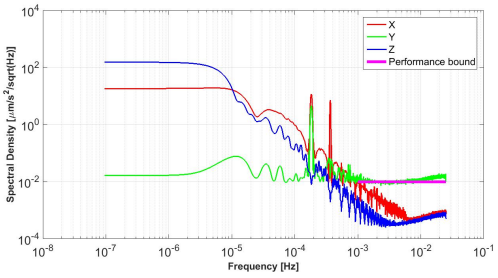

Fig. 5. Simulated PSD of the non-gravitational residuals.

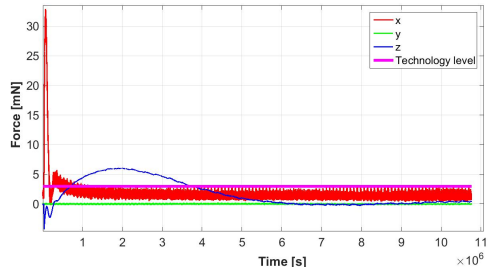

Fig. 6. Simulated total linear command.

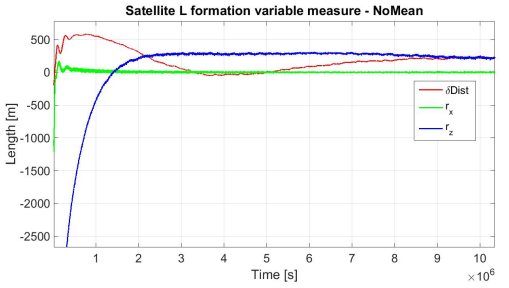

Fig. 7. Simulated time profile of the formation variable perturbations (formation mean tracking errors).

formation command. The total longitudinal component (x, in red) includes the longitudinal drag compensation that becomes the largest component when formation transient vanishes. After a transient of about two weeks, the command peak is below 3 mN, a value which is deemed compatible with expected thruster technology level. The transient behavior is linked to the linear residuals, and the control gains; as shown from the simulated results. We have confidence that an optimal combined tuning of the control gains may reduce both the duration and the peak of the transient phase. However, trying to reduce this peak value as well as the transient time constant was beyond the scope of this study and will represent a natural prosecution of this work. Finally, Fig. 7 depicts the formation triangle position variables time history (distance δd, mean altitude r_z and formation mean radius deviation r_x) with respect to their reference values. All the variables stay considerably within the bound that corresponds to the fractional requirement in Table 1.

6. CONCLUSION

In summary, we have presented an enhanced version of the integrated formation control design (Canuto et al. (2014a)) which has been conceived to meet the formation and drag-free requirements of the Next Generation Gravity Missions, under study by ESA. This design is based on the innovative concepts of formation triangle and formation local orbital frame (FLOF). This enhanced multi-rate and multi-hierarchical control architecture has been studied to overcome the possible weakness concerning the formation stability in some orbital conditions, experienced in the previous study. Extensive high-fidelity simulation runs proved the control architecture validity and showed that the enhanced control strategy is capable of keeping the formation variables stable within the required band, all over the 10-year mission, through a low-thrust authority in the order of few milli-newtons.

REFERENCES

Alfriend, K.T., Gim, D.W., and Schaub, H. (2000). Gravitational perturbations, nonlinearity and circular orbit assumption effects on formation flying control strategies. *Guidance and control 2000*, 139–158.

Canuto, E., Colangelo, L., Buonocore, M., Massotti, L., and Girouart, B. (2014a). Orbit and formation control for low-earth-orbit gravimetry drag-free satellites. *Proceedings of the Institution of Mechanical Engineers, Part G: Journal of Aerospace Engineering*, 229(7), 1194–1213. doi:10.1177/0954410014548236.

Canuto, E., Montenegro, C.P., Colangelo, L., and Lotufo, M. (2014b). Active Disturbance Rejection Control and Embedded Model Control: A case study comparison. In *Proceedings of the 33rd Chinese Control Conference*, 3697–3702. IEEE. doi:10.1109/ChiCC.2014.6895554.

Canuto, E., Montenegro, C.P., Colangelo, L., and Lotufo, M. (2014c). Embedded Model Control: Design separation under uncertainty. In *Proceedings of the 33rd Chinese Control Conference*, 3637–3643. IEEE. doi:10.1109/ChiCC.2014.6895544.

Guibout, V.M. and Scheeres, D.J. (2012). Spacecraft Formation Dynamics and Design. *Journal of Guidance, Control, and Dynamics*. URL `http://arc.aiaa.org/doi/abs/10.2514/1.13002`.

Inalhan, G., Tillerson, M., and How, J.P. (2002). Relative Dynamics and Control of Spacecraft Formations in Eccentric Orbits. *Journal of Guidance, Control, and Dynamics*, 25(1).

Melton, R.G. (2000). Time-Explicit Representation of Relative Motion Between Elliptical Orbits. *Journal of Guidance, Control, and Dynamics*, 23(4), 604–610. doi:10.2514/2.4605.

Ren, W. and Beard, R.W. (2004). Formation feedback control for multiple spacecraft via virtual structures. doi:10.1049/ip-cta:20040484.

Schaub, H. and Alfriend, K.T. (2000). Invariant Relative Orbits for Spacecraft Formations.

Schaub, H., Vadali, S.R., Junkins, J.L., and Alfriend, K.T. (2000). Spacecraft Formation Flying Control Using Mean Orbit Elements. *Journal of the Astronautical Sciences*. doi:10.2514/2.4774.

Wiltshire, R.S. and Clohessy, W.H. (1960). Terminal guidance system for satellite rendezvous. *Journal of the Aerospace Sciences*, 27(9), 653–658,674. doi:10.2514/8.8704.

Yamanaka, K. and Ankersen, F. (2002). New State Transition Matrix for Relative Motion on an Arbitrary Elliptical Orbit. *Journal of Guidance, Control, and Dynamics*, 25(1), 60–66. doi:10.2514/2.4875.